JACS
JOURNAL OF THE AMERICAN CHEMICAL SOCIETY
Article
pubs.acs.org/JACS

Experimental and Theoretical Comparison of Gas Desorption Energies on Metallic and Semiconducting Single-Walled Carbon Nanotubes

Lynn Mandeltort,[†] De-Li Chen,[‡] Wissam A. Saidi,[‡] J. Karl Johnson,*[,‡,§] Milton W. Cole,[∥] and John T. Yates, Jr.*[,†]

[†]Department of Chemistry, University of Virginia, Charlottesville, Virginia 22904, United States
[‡]Department of Chemical and Petroleum Engineering, University of Pittsburgh, Pittsburgh, Pennsylvania 15261, United States
[§]National Energy Technology Laboratory, Pittsburgh, Pennsylvania 15236, United States
[∥]Department of Physics, Penn State University, University Park, Pennsylvania 16802, United States

ABSTRACT: Single-walled carbon nanotubes (SWNTs) exhibit high surface areas and precisely defined pores, making them potentially useful materials for gas adsorption and purification. A thorough understanding of the interactions between adsorbates and SWNTs is therefore critical to predicting adsorption isotherms and selectivities. Metallic (M-) and semiconducting (S-) SWNTs have extremely different polarizabilities that might be expected to significantly affect the adsorption energies of molecules. We experimentally and theoretically show that this expectation is contradicted, for both a long chain molecule (*n*-heptane) and atoms (Ar, Kr, and Xe). Temperature-programmed desorption experiments are combined with van der Waals corrected density functional theory, examining adsorption on interior and exterior sites of the SWNTs. Our calculations show a clear dependence of the adsorption energy on nanotube diameter but not on whether the tubes are conducting or insulating. We find no significant experimental or theoretical difference in adsorption energies for molecules adsorbed on M- and S-SWNTs having the same diameter. Hence, we conclude that the differences in polarizabilities between M- and S-SWNTs have a negligible influence on gas adsorption for spherical molecules as well as for highly anisotropic molecules such as *n*-heptane. We expect this conclusion to apply to all types of adsorbed molecules where van der Waals interactions govern the molecular interaction with the SWNT.

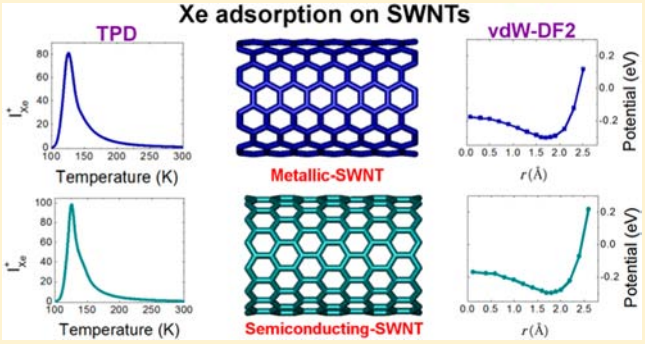

1. INTRODUCTION

It is widely known that single-walled carbon nanotubes (SWNTs) exist as either metallic or semiconducting entities and that the electronic structure of a SWNT is determined by its chiral indices (n, m).[1,2] Metallic SWNTs (M-SWNTs) have chiral indices such that $n = m$ and extremely large longitudinal polarizabilities, whereas semiconducting SWNTs (S-SWNTs), which have $n - m = j$, where j is not an integral multiple of 3, have much smaller longitudinal polarizabilities that are proportional to the radius (and thus the number of atoms) and inversely proportional to the square of the band gap, according to the density functional perturbation theory based calculations of Kozinsky et al.[3,4] On the other hand, transverse polarizabilities of SWNTs are found to be relatively insensitive to the chirality and longitudinal band structure. Experimentally, many observations indicate differences between S- and M-SWNTs. For example, Lu et al.[5] reported the first measurement of the near-dc polarization of an individual SWNT and found evidence for a difference in the longitudinal dielectric property between S- and M-SWNTs. Yanagi et al.[6] found significant differences in the charge transport mechanisms between S- and M-SWNTs. From a theoretical standpoint, it has been shown that there are dramatic differences in the van der Waals (vdW) interactions between pairs of S- or M-SWNTs when the nanotubes are parallel and held at distances large compared with the diameter of the nanotubes.[7,8]

It is reasonable to presume that the interaction potential of gas molecules with the interior and exterior adsorption sites of SWNTs would be sensitive to differences in the polarizabilities of the S- and M-SWNTs. This is because the vdW dispersion coefficients between two particles are proportional to their polarizabilities. Molecular adsorption of gases on SWNTs has been widely studied.[9−16] Some of these studies provide evidence for differences between adsorption on S- and M-SWNTs. Theoretical calculations by Jhi et al.[9] indicate that the weak coupling between adsorbed O_2 and the S-SWNT leads to a small charge transfer of 0.1 electron from SWNT to O_2 and the appearance of conducting states near the band gap that change the electronic structure of the SWNT. Similarly, NO_2

Received: March 22, 2013
Published: April 29, 2013

and NH_3 act as charge acceptors and donors, respectively, to SWNTs, and therefore, their adsorption significantly changes the electrical properties of S-SWNTs.[10] Some large organic and organometallic molecules that physically adsorb on SWNTs were found to respond differently to S- and M-SWNTs,[14,15] where the interactions consist of both a vdW energy and a charge transfer energy. Other theoretical investigations showed very small energy differences for small molecule adsorption on S- and M-SWNTs.[10,13,16] However, most previous theoretical results are based on local or semilocal density approximation calculations, where the long-range dispersion energy is missing or not calculated accurately. Hence, these previous calculations cannot be considered definitive.

There are several challenges associated with resolving the differences between the interaction of S- and M-SWNTs with adsorbates, from both experiment and theory. Experimentally, obtaining sufficiently large quantities of pure S- and M-SWNTs for measuring the adsorption energies has been possible only recently, thanks to the work of Hersam et al.,[17,18] who separated S- and M-SWNTs using a density differentiation method. Most previous theoretical studies on adsorbate/SWNT systems have used local density approximation theory, which is unreliable for describing vdW dispersion interactions that are ubiquitous for these interactions.[19,20] Møller−Plesset perturbation theory diverges for metallic systems and thus is not suitable for investigating M-SWNTs. Quantum Monte Carlo and random phase approximation methods are able to reproduce vdW energies but are computationally very expensive.[21−23] Recently developed methods for including vdW interactions within density functional theory (DFT), such as the vdW-DF approach of Langreth and co-workers[24−26] and the Tkatchenko and Scheffler vdW-TS[27,28] method, do not completely capture many-body effects and thus cannot explicitly capture the many-body polarization expected for metallic systems. Nevertheless, these methods have been shown to be accurate for describing interactions of noble gases with metal surfaces,[19,20] H_2 on the Cu(111) surface,[29] and H_2O with graphene.[30]

We recently used a combined approach including experiments and vdW-corrected DFT to study the binding energy of Xe adsorbed on S- and M-SWNTs.[31] We found that binding energies derived from temperature-programmed desorption (TPD) experiments for Xe on samples of purified S- and M-SWNTs are almost identical, indicating that the vdW interactions between Xe and SWNTs are insensitive to the difference in electronic structure of these nanotubes. We also found that our calculated vdW-DF2[26] and vdW-TS[27] adsorption energies on M- and S-SWNTs agree well with measured desorption energies. Our calculations show that adsorption energies for Xe on the interior and exterior of SWNTs depend critically on the diameter of the nanotube but not on the metallic or semiconducting nature of the SWNTs.[31]

As pointed out in our previous paper,[31] the insensitivity of Xe-SWNT adsorption energies to the conductivity of the SWNTs may be rationalized by noting that Xe can be considered as a pointlike object and it has been shown that pointlike objects (such as atoms) do not give rise to the unconventional vdW interactions observed for parallel M-SWNTs at large distances.[7,8] However, it is possible that highly *anisotropic* molecules and polar molecules exhibit significant differences in adsorption energies on S- and M-SWNTs that are not seen for noble gases. In this paper, we use experiment and theory to study the adsorption of *n*-heptane, a highly anisotropic molecule, on S- and M-SWNTs. We also present predictions for a series of noble gases (Ar, Kr, and Xe) on six SWNTs, three metallic and three semiconducting.

2. EXPERIMENTAL AND THEORETICAL DETAILS

2.1. Ultrahigh Vacuum Apparatus and SWNT Materials. The separated S- and M-SWNT samples used in these studies were commercial samples prepared by arc discharge and separated using propriety surfactants and density gradient centrifugation.[32] The S- and M-SWNT solutions have quite different optical absorption spectra in the visible region, as shown in Figure 1.

Figure 1. Separated SWNT solutions. (left) S-SWNTs; (right) M-SWNTs.

A mixture of nanotube types prepared by the Smalley group by laser ablation[33] was also studied, having been purified by oxidative acid treatment[34] and suspended in dimethyl formamide (DMF). Adsorption of gases on this mixture of nanotube types has been extensively studied, as summarized by Kondratyuk and Yates,[35] and therefore serves as a reference sample against which to compare our results on M- and S-SWNTs. A summary of the three samples investigated experimentally is presented in Table 1. The nanotubes in these samples have a range of diameters from 12 to 17 Å, with an average diameter of 14 Å.

Table 1. Comparison of SWNT Samples Used in This Study

sample	synthesis	solvent	av diameter
S-SWNTs	arc discharge	water/ionic surfactant(s)[a]	14 Å
M-SWNTs	arc discharge	water/ionic surfactant(s)[a]	14 Å
mixed SWNTs	laser ablation	DMF	14 Å

[a]Proprietary surfactants are not specified in the manufacturer's data sheet.

The samples were prepared for ultrahigh vacuum (UHV) studies by drop-depositing microliter aliquots of the suspensions onto clean gold plates that are heated to 80 °C to rapidly evaporate the solvents, resulting in nanotube deposits that covered a surface area of ∼1 cm^2 on the gold plate. The mass of the each SWNT sample was ∼30 μg. By using a nominal surface area of 1000 $m^2\ g^{-1}$ for SWNTs,[36] the surface area of the samples studied exceeded 100 cm^2.

Nanotubes were inserted together as two separate samples, each on a Au support plate in a UHV chamber equipped with a turbo pump, an ion pump, and a titanium sublimation pump to maintain a base pressure of 2×10^{-10} Torr. The experimental setup has been discussed in more detail by Kondratyuk and Yates.[37] The nanotubes were heat treated in UHV in stages, from room temperature up to 373 K, and then in 100 K increments up to 1073 K. Desorption of material was monitored as the samples were heated, and TPD of Xe and heptane was performed after each heat treatment. It was noted that iodine (m/z = 127) was evolved up to ∼900 K and then ceased evolution upon higher temperature heating. Iodine is a component of the density gradient separation media, which includes iodoxanol.[17]

Adsorption on the SWNT samples was carried out using a collimated microcapillary array doser[38] designed to deliver an accurately known flux of molecules to the samples. The permeances

dx.doi.org/10.1021/ja402928s | J. Am. Chem. Soc. 2013, 135, 7768−7776

employed were 5.4×10^{12} and 6.2×10^{12} molecules $Torr^{-1}$ cm^{-2} s^{-1} for Xe and *n*-heptane, respectively. The exposure was controlled by dosing the samples for a given time at a fixed gas delivery pressure behind a pinhole aperture located inside the doser structure. For exposures of less than 5×10^{14} molecules cm^{-2}, a pressure of 1 Torr was used, while a pressure of 8 Torr was used for higher exposures. The corrected Xe adsorption temperatures were 101.5 and 100.0 K for the M-SWNT and S-SWNT samples, respectively. The corresponding adsorption temperatures for *n*-heptane were 121.5 and 120.0 K (see Section 2.2).

TPD experiments were conducted with a heating rate of 2 K s^{-1} and utilized a proportional-integral-derivative (PID) controller to produce linear temperature ramps. Desorbing molecules were detected with an apertured quadrupole mass spectrometer (QMS, UTI-100C) designed for line-of-sight detection of desorbing molecules. Before each desorption experiment, the QMS was calibrated against a background of gas supplied by the doser delivering a known flux to the chamber. All TPD spectra were corrected for small changes in the QMS sensitivity. Xenon from Matheson and *n*-heptane from J. T. Baker were used after being purified by several freeze–pump–thaw cycles. Peak temperatures for thermal desorption were measured by numerical differentiation of the desorption data.

2.2. Temperature Scale Calibration. The results of these studies rely heavily on careful temperature measurements of two separately supported samples. That is, any measured temperature difference must be correctly attributed to differences in the SWNT samples and must *not* be due to an inherent or systematic discrepancy in temperature scale measurements between the support plates. Thus, many experiments were performed on the clean Au plates prior to and after depositing the SWNTs to establish the magnitude and reproducibility of any temperature scale differences.

In order to accurately compare the temperature scales for each sample plate, we employed as a thermometer a multilayer of *n*-heptane on the SWNT samples, where the term "multilayer" refers to the condensation of many layers beyond the monolayer, the desorption of which displays zero-order kinetics. The zero-order desorption kinetics characteristic of sublimation from the *n*-heptane multilayer provide a very accurate temperature scale independent of the interaction of the molecule with the underlying SWNT sample and Au support plate. The leading edge of the thermal desorption trace is sensitively controlled by temperature and follows the Clausius–Clapeyron equation accurately.[39] Figure 2a shows a logarithmic plot of the *n*-heptane desorption signal for both samples versus $1/T$ and is sufficiently linear in the region above $1/T = 0.006$ K^{-1} until noise becomes a significant factor for $1/T > 0.007$ K^{-1}.

A small temperature offset of ΔT is present in the *n*-heptane desorption from the two sample plates, as can be seen from the enlarged inset shown in Figure 2b. By adding this offset temperature (ΔT) to the data from the metallic SWNT sample and least-squares fitting the points from both data sets (Figure 2c), it may be seen that the sample Pearson correlation coefficient, r_P, passes through a minimum at $\Delta T = 1.5$ K. Thus, adding a correction of 1.5 K to desorption measurements made for the M-SWNT sample will accurately reconcile the temperature scales. This correction was checked by another method involving characteristic desorption peak temperatures for *n*-heptane from the uncovered (no SWNTs) Au plates. This approach showed that ΔT could range from about 1.0 to 2.3 K over the course of many experiments. We have applied a uniform +1.5 K correction to the temperature scale used for the M-SWNT sample, and we estimate that our corrected temperature scales on the two samples agree within ±0.8 K. The value of the heat of sublimation for a multilayer of *n*-heptane calculated from the data in Figure 2c is 58.2 ± 0.7 kJ mol^{-1} from both samples when the 1.5 K temperature correction is included. This compares favorably with the literature value of 57.9 kJ mol^{-1}.[40]

2.3. Computational Details. We model the gas adsorption on isolated infinitely long (periodic) SWNTs in order to capture the true metallic nature of the SWNTs that would be challenging to capture using cluster models (insofar as cluster models involve purely localized states). The computational details have been described in our previous paper.[31] Briefly, we employ the van der Waals density functional (vdW-DF) approach,[24−26] specifically using the vdW-DF2,[26] as well as the Tkatchenko and Scheffler vdW-TS scheme,[27,28] to describe vdW interactions. The vdW-TS scheme has been implemented in the Vienna ab initio simulation package[41−44] (VASP) by Al-Saidi et al. and was applied in the study of a variety of extended and isolated systems.[28] The vdW-DF2 calculations of noble gas adsorption on SWNTs were carried out using an in-house modified version of VASP,[19,20] while vdW-DF2 data for *n*-heptane relaxation on SWNTs were obtained using a different implementation available in VASP.[45] These codes give very similar results.

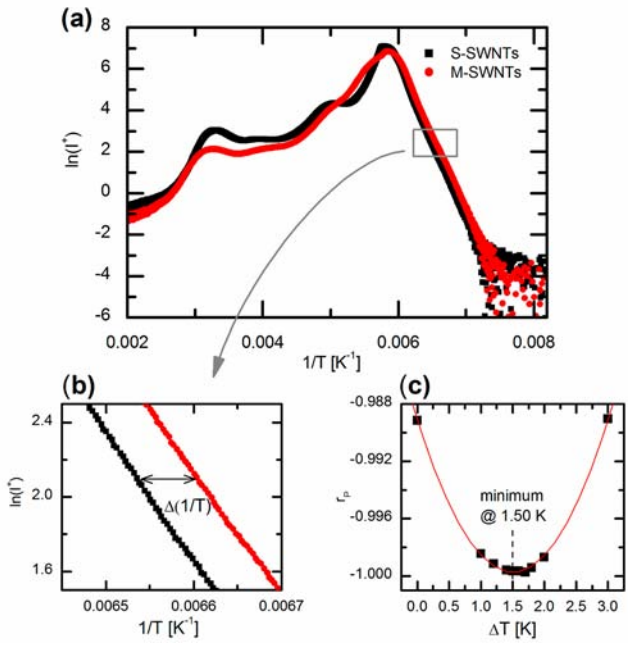

Figure 2. (a) Logarithmic plot of the intensity of *n*-heptane desorption from the S- and M-SWNT samples. The linear region corresponds to the leading edge of the zero-order kinetic desorption from a multilayer thickness of *n*-heptane (*n*-heptane exposure = 7.4×10^{16} molecules cm^{-2}). (b) Enlarged $1/T$ scale, showing displacement of a section of the zero-order kinetic curve. (c) Least-squares fit of the composite data showing minimization of the standard Pearson correlation coefficient, r_P, for the two sets of data for a correction factor of $\Delta T = 1.5$ K.

We used a supercell approach with two or three unit cells for S- and M-SWNTs, respectively. The length of a unit cell along the tube axis is 4.26 Å for (*n*, 0) S-SWNTs and 2.46 Å for (*n*, *n*) M-SWNTs. We used four and seven unit cells for S- and M-SWNTs in our *n*-heptane calculations. A vacuum spacing of at least 15 Å in the directions perpendicular to the nanotube axis was used to mitigate interactions with periodic images. The Brillouin zone was sampled using Monkhorst–Pack[46] grids of $1 \times 1 \times 3$ and $1 \times 1 \times 1$ for the noble gas and *n*-heptane systems, respectively. We employed a planewave energy cutoff of 600 eV for the noble gas calculations and a smaller cutoff of 400 eV for the *n*-heptane study (due to its large system size). We estimate the precision of the calculated desorption energies to be better than 0.01 eV, based on the convergence with respect to the vacuum spacing, energy cutoff, Brillouin zone sampling, and Xe lateral interaction. The accuracy of our calculations can perhaps be estimated from the differences between the vdW-DF2 and vdW-TS results, which in our calculations for *n*-heptane are roughly 20%. The effects of the SWNT diameter on the adsorption energies were explored using three pairs of metallic armchair (*n*, *n*) and semiconducting zigzag (*n*, 0) SWNTs having radii that are very similar for each pair. The smallest SWNTs used in our calculations are (10, 0) and (6, 6), with radii of 3.9 and 4.1 Å, respectively. The next set of SWNTs are (14, 0) and (8, 8), having radii of 5.5 and 5.4 Å, respectively. The largest SWNTs are (20, 0) and (12, 12), with radii of 7.8 and 8.1 Å, respectively. Note that

dx.doi.org/10.1021/ja402928s | J. Am. Chem. Soc. 2013, 135, 7768−7776

we have chosen $(n, 0)$ nanotubes such that n is not an integer multiple of 3 to ensure that the zigzag SWNTs have appreciable band gaps.

3. RESULTS AND DISCUSSION

3.1. Studies of *n*-Heptane Desorption from M- and S-SWNTs. One of the main goals of this work was to test whether the binding energies of highly anisotropic molecules to S- and M-SWNTs are significantly different. Accordingly, we have performed TPD experiments using *n*-heptane as the adsorbate. Figure 3 shows the desorption of increasing quantities of *n*-heptane from M-, S-, and mixed-SWNTs. The fingerprint pattern known for long chain alkanes desorbing from SWNTs is readily apparent on all of the samples,[35,47] where four unique desorption states (A: interior site; B: groove site; C: exterior site; and D: multilayer desorption state) are clearly observed.

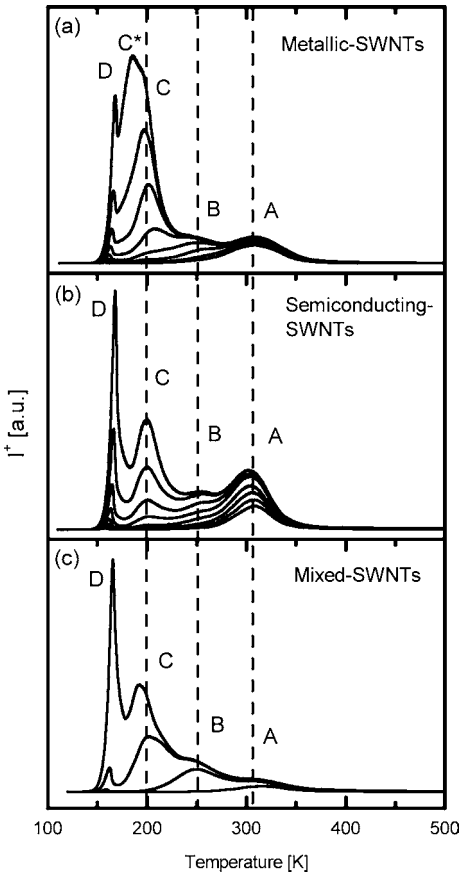

Figure 3. Comparison of *n*-heptane thermal desorption from (a) M-SWNTs, (b) S-SWNTs, and (c) mixed-SWNTs. The sequence of binding states, A, B, C, and D, is similar on all three samples, producing a fingerprint pattern. See the text for definition of states. State C* may be related to an impurity site on M-SWNTs. The different curves in each graph correspond to different *n*-heptane exposures.

The fingerprint pattern shown in Figure 3c reveals four binding states for *n*-heptane. State A corresponds to *n*-heptane desorbing from interior sites; state B corresponds to desorption from groove sites between bundles of SWNTs; state C corresponds to desorption from the outer surfaces of SWNTs; state D corresponds to multilayer *n*-heptane desorption from the sample.[35,47] It has been shown that the capacity of linear groove sites to adsorb *n*-alkanes scales inversely as the length of the alkane (as expected intuitively, since the molecules nestle collinearly at maximum packing along the groove).[47] Furthermore, it has been found that molecules can be displaced from one SWNT site to another by processes involving molecules having higher binding energies.[48] It has also been found that molecules in the interior sites (A) are shielded from reactions from gas-phase atomic hydrogen,[49] which serves as an independent check that the A sites are indeed inside the nanotube.

It is remarkable that the TPD profiles of Figure 3 obtained from the separated M-SWNTs and S-SWNTs produced via an entirely different synthesis method and prepared from a distinctly dissimilar solvent/surfactant dispersion method are so similar to those of the mixed-SWNTs. The resemblance among the three samples of SWNTs shown in Figure 3 indicates that the four binding states of *n*-heptane exist on all three samples, with some small differences in state population and desorption energy. The S-SWNT sample closely corresponds to the mixed-SWNT sample. The M-SWNT sample displays an additional adsorption state designated C* with a desorption temperature just below that of state C. State C* may correspond to *n*-heptane desorption from impurities that remain behind on the M-SWNT sample.

The values of T_{peak} for *n*-heptane desorption states A, B, and C (Table 2) are very close to each other, with a difference that is less than 9 K for all cases, indicating that the energetics for *n*-heptane desorption are highly similar for all three types of SWNTs. From consideration of the factors controlling the shape of TPD curves, it is known that the value of T_{peak} is an accurate measure of the temperature where the instantaneous desorption rate equals the rate of pumping from the vacuum system. Since the rate of pumping is constant, the value of T_{peak} corresponds to a constant rate of desorption on all three samples and may therefore be used for comparison.[50] For first-order thermal desorption kinetics, T_{peak} will be constant with coverage if the desorption energy is coverage independent. This is seen to be the case in Figure 3.

Table 2. Peak Temperatures Measured from TPD Experiments, Shown in Figure 3[a]

site	M-SWNT	S-SWNT	mixed
A	310 K	306 K	315 K
B	252 K	253 K	250 K
C	197 K	199 K	202 K

[a]The labels A, B, and C are the same as those in Figure 3.

We have computed the binding energies of *n*-heptane on two sets of SWNTs having similar radii, that is, (8, 8)/(14, 0) and (12, 12)/(20, 0). We used two different vdW-corrected DFT methods, vdW-DF2 and vdW-TS. The optimized structures of the *n*-heptane/(20, 0) SWNT system for exterior and interior adsorption are shown in Figure 4. The calculated desorption energies are listed in Table 3. Note that the desorption energies computed from vdW-DF2 are about 15−18% smaller than those computed from vdW-TS. However, the energy differences between tubes of similar sizes are very similar, and the ratios of energies for tubes of different sizes are also nearly identical for the two different DFT methods. The maximum difference in energies between M- and S-SWNTs having similar diameters is 40 meV. Thus, we conclude there is essentially no difference between desorption energies of *n*-heptane on M- and S-SWNTs. This is consistent with the experimentally measured T_{peak} values.

dx.doi.org/10.1021/ja402928s | J. Am. Chem. Soc. 2013, 135, 7768−7776

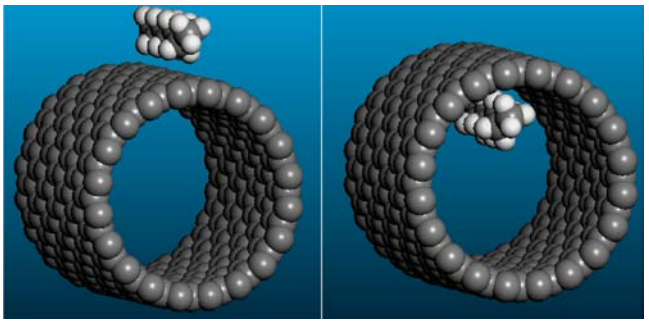

Figure 4. Optimized structure of *n*-heptane on the (left) exterior and (right) interior sites of a (20, 0) SWNT.

Table 3. Desorption Energies (in eV) for *n*-Heptane on Two Pairs of SWNTs for Interior (E_{des}^{in}) and Exterior (E_{des}^{ex}) Sites, Calculated from vdW-DF2 and vdW-TS Methods

		vdW-DF2		vdW-TS	
SWNT	type	E_{des}^{in}	E_{des}^{ex}	E_{des}^{in}	E_{des}^{ex}
(8, 8)	M	1.07	0.43	1.31	0.54
(14, 0)	S	1.08	0.42	1.27	0.51
(12, 12)	M	0.75	0.41	0.88	0.48
(20, 0)	S	0.72	0.40	0.88	0.49

Our calculations show that the *n*-heptane desorption energies are significantly affected by both SWNT diameter and identity of the sites (exterior or interior). The smaller SWNTs have much larger desorption energies for interior sites than SWNTs with larger diameter, as expected. For example, the difference between the interior desorption energies for the (8, 8) and (12, 12) SWNTs is 0.32 eV as computed by vdW-DF2, indicating the desorption energy of *n*-heptane at the interior site of the SWNT is very sensitive to the diameter of SWNTs. The desorption energies for *n*-heptane at exterior sites are much smaller than those for interior sites. For example, the difference between the interior and exterior desorption energies for the (14, 0) and (20, 0) SWNTs are 0.66 and 0.32 eV, respectively, as computed from vdW-DF2. The trends computed from the vdW-TS method are the same.

The Redhead equation is commonly used to estimate the energy of desorption from the measured T_{peak} values. The Redhead equation for first-order desorption kinetics is given by[51]

$$E_{des} = k_B T_{peak} \ln\left(\frac{\nu k_B T_{peak}^2}{\beta E_{des}}\right) \quad (1)$$

where E_{des} is the desorption energy, k_B is the Boltzmann constant, ν is the preexponential factor (in s^{-1}), and β is the heating rate (in K s^{-1}). It is common to assume a value of the prefactor for simple molecules of $\nu = 10^{13}$ s^{-1}. This value is based on statistical mechanical arguments. The value of ν can be estimated experimentally through the use of a range of heating rates.[39] Prefactor values for *n*-heptane desorbing from graphite have been reported to be about 10^{17} to 10^{19} s^{-1}.[52−55] Direct comparison of the experimentally measured T_{peak} values and the calculated binding energies for *n*-heptane on SWNTs is hampered by the lack of available prefactor values for the *n*-heptane/SWNT system. Use of prefactors measured for planar graphite is not warranted because graphite is very different from the cylindrical SWNTs that form a tangled mat from which *n*-heptane must desorb. We have therefore calculated values of ν from our vdW-corrected DFT data and the experimentally measured T_{peak} values (Table 2) through a Redhead analysis[51] using eq 1. We found that the predicted prefactor changes dramatically with the diameter of the SWNTs (from 10.8 to 16.2 Å) and with the DFT method. The calculated prefactors for interior desorption (site A in Table 2) range from 10^{13} to 10^{19} s^{-1} for vdW-DF2 and from 10^{16} to 10^{23} s^{-1} for vdW-TS energies. Prefactors for desorption from the exterior site C have smaller ranges, from 10^{11} to 10^{12} s^{-1} and from 10^{13} to 10^{15} s^{-1} for vdW-DF2 and vdW-TS energies, respectively.

3.2. Adsorption of Noble Gases on M- and S-SWNTs.

Xenon was also used to probe vdW adsorption differences on the M- and S-SWNTs. Figure 5 shows the desorption of Xe from the SWNTs, which had been previously activated to 1073 K. We note that the desorption peak temperatures for the M- and S-SWNTs shown in Figure 5 at similar coverages are remarkably similar, with differences less than 1 K, as determined by the derivatives of the TPD traces (Figure 5 insets). The values of T_{peak} can be converted to E_{des} using eq 1 and assuming a typical value of $\nu = 10^{13}$ s^{-1} for the prefactor for first-order desorption of Xe from the two SWNT samples. The average desorption energies measured from three independent experiments are identical to within experimental uncertainty for S- and M-SWNTs, both giving 0.334 ± 0.002 eV. The data in Figure 5 show that the full width at half-maximum is about 30% greater for Xe/M-SWNTs than for Xe/S-SWNTs. We believe this may be due to residual impurities present on the M-SWNTs in excess of those found on S-SWNTs.

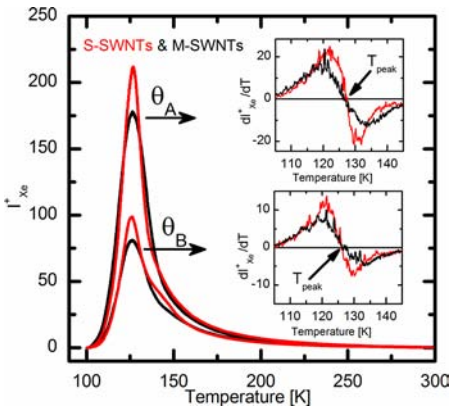

Figure 5. TPD of Xe from M-SWNTs (black curves) and S-SWNTs (red curves) activated to 1073 K at two different coverages, θ. $T_{exposure}$ for M-SWNTs = 101.5 K; $T_{exposure}$ for S-SWNTs = 100 K; exposure ≤ 4.0×10^{16} cm^{-2}; $dT/dt = 2$ K s^{-1}. The peak temperatures, T_{peak}, correspond to the points where the derivatives of the TPD curves go to zero. The calculated derivatives, shown in the insets, have been smoothed with five point adjacent averaging.

We have computed the potential energy curves for Ar, Kr, and Xe from vdW-DF2 for adsorption on the interior and exterior of the three pairs of S- and M-SWNTs identified above. Previous studies[56−58] have shown that noble gases energetically prefer hollow sites (hexagon sites) over low-coordination sites on graphite and graphene. Our calculations indicate that the same is true for adsorption on SWNTs. For example, the potential energy curves for Ar adsorption on a (10, 0) SWNT at hollow (H) and atop (A) sites are shown in Figure 6. The hollow site is favored over the atop site by 11 meV, as computed from vdW-DF2. The equilibrium distance from the

dx.doi.org/10.1021/ja402928s | J. Am. Chem. Soc. 2013, 135, 7768−7776

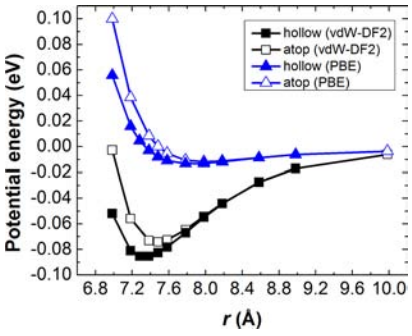

Figure 6. Comparison of the calculated potential energies for Ar at atop and hollow sites on the exterior of a (10, 0) nanotube, as a function of distance from the SWNT axis, *r*, as computed from PBE and vdW-DF2.

surface for atop site adsorption is 3.5 Å, which is slightly larger than 3.3 Å at the hollow site and consistent with larger adsorption energy at the hollow site. We have computed the vibrational frequencies for Ar at the atop site of a (10, 0) SWNT and have found that the atop site is a saddle point of index 2, that is, Ar on the atop site has eigenvectors with two imaginary frequencies. Therefore, the calculations in the remainder of the paper deal only with hollow site adsorption. The PBE functional also predicts that the hollow site is favored, but with a binding energy of about 1 meV, compared with 85 meV as computed from vdW-DF2 (Figure 6). This is similar to the situation for noble gases adsorbed on metal surfaces, where PBE also predicts the correct binding site (atop in that case) but dramatically underestimates the binding energy.[19,20] The fact that PBE captures the correct binding site in the present case is somewhat surprising, because on metal surfaces the atop site is lower in energy than the hollow site due to a balance between electrostatic and kinetic energies,[19,20] whereas vdW interactions dominate for the adsorbate/SWNT systems studied here.

The potential energy curves for Ar, Kr, and Xe on three pairs of M- and S-SWNTs on both interior and exterior sites computed from vdW-DF2 are presented in Figure 7a–f. We can see that the potential energy curves of noble gases on M- and S-SWNTs having about the same radii are very similar. The desorption energies, taken as the negative of the adsorption (binding) energies or minimum of the potential energies (Figure 7), and the equilibrium distances are summarized in Table 4. The striking result from Figure 7 and Table 4 is that desorption energies for Ar, Kr, and Xe on SWNTs are insensitive to whether the tubes are metallic or semiconducting. The exterior and interior desorption energies for each metallic and semiconducting pair of SWNTs having nearly the same radii are almost identical. We see from Table 4 that the desorption energies decrease from Xe to Kr to Ar, following the polarizabilities of the noble gases, as expected. From Table 4, we also notice that the difference between interior and exterior desorption energies is the largest for the smallest SWNT and the difference becomes smaller as the diameter of SWNTs becomes larger. The ratio $E_{des}^{in}/E_{des}^{ex}$ decreases from 5.2 to 2.6 to 1.7, for Xe on (10, 0), (14, 0), and (20, 0), respectively.

We can compare our calculated desorption energies for Xe with the experimentally measured desorption energies by noting that the average diameter of the SWNTs used in experiments, 14 Å, lies between the medium (~11 Å) and largest (~16 Å) SWNTs studied in the simulations. The Xe desorption energies for Xe from the interior sites of these SWNTs range from 0.30 to 0.22 eV (Table 4). These values are in reasonably good agreement with the experimental result of 0.334 ± 0.002 eV.

In contrast to the *n*-heptane results discussed above, differences between the desorption energies on interior and exterior sites for Xe on the medium and large diameter SWNTs are much smaller. Taking the (20, 0) SWNT for example, we find that the exterior adsorption site is only 0.09 eV less favorable than the interior site for Xe (Table 4), compared with a difference of 0.32 eV for *n*-heptane (vdW-DF2, Table 3). This helps to explain why the TPD spectra for *n*-heptane can resolve

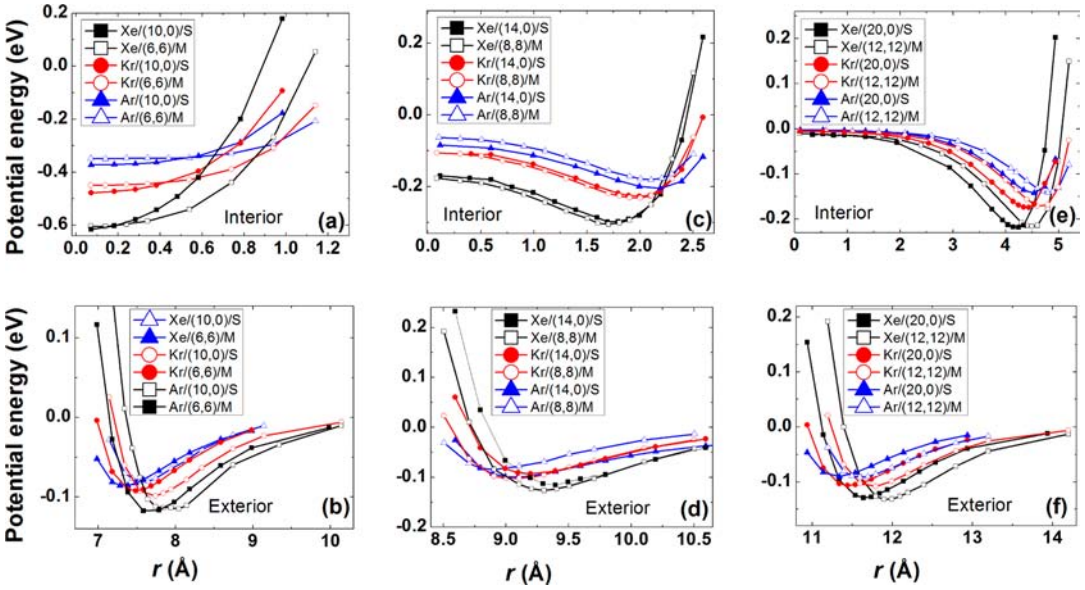

Figure 7. Comparison of potential energies (in eV) computed from vdW-DF2 for Ar, Kr, and Xe adsorption on (a) interior and (b) exterior sites of (10, 0) and (6, 6) SWNTS, (c) interior and (d) exterior sites of (14, 0) and (8, 8) SWNTs, and (e) interior and (f) exterior sites of (20, 0) and (12, 12) SWNTs, as a function of the distance, *r*, from the axis of the nanotube.

dx.doi.org/10.1021/ja402928s | J. Am. Chem. Soc. 2013, 135, 7768–7776

Table 4. Desorption Energies (eV) for Interior, E_{des}^{in}, and Exterior, E_{des}^{ex}, Sites and Adsorption Distances, r (Å), from the Axis of the SWNTs as Computed from vdW-DF2[a]

		Ar				Kr				Xe			
SWNT/type	R	E_{des}^{in}	r	E_{des}^{ex}	r	E_{des}^{in}	r	E_{des}^{ex}	r	E_{des}^{in}	r	E_{des}^{ex}	r
(6, 6)/M	4.1	0.35	0.0	0.08	7.6	0.45	0.0	0.10	7.7	0.60	0.0	0.12	8.0
(10, 0)/S	3.9	0.37	0.0	0.09	7.4	0.48	0.0	0.10	7.5	0.62	0.0	0.12	7.7
(8, 8)/M	5.4	0.19	2.1	0.09	8.9	0.23	2.0	0.10	9.0	0.30	1.7	0.13	9.3
(14, 0)/S	5.5	0.18	2.2	0.08	9.1	0.23	2.0	0.09	9.2	0.30	1.7	0.12	9.4
(12, 12)/M	8.1	0.14	4.8	0.09	11.6	0.17	4.6	0.11	11.8	0.22	4.5	0.13	11.9
(20, 0)/S	7.8	0.14	4.5	0.09	11.3	0.17	4.4	0.11	11.4	0.22	4.2	0.13	11.6

[a]The radii of the SWNTs, R (Å), are also given.

the different adsorption sites, whereas the Xe TPD data cannot resolve different sites; the much greater difference in binding energies for *n*-heptane on the interior and exterior sites allows for the higher resolution in the TPD spectra. We note that the lower coverages used in this work are not expected to occupy all available sites, unlike the work of Ulbricht, who saw peaks for the groove and exterior sites while performing TPD starting from a lower temperature (<60 K) using higher coverages and a slower heating rate (0.5 K s^{-1}).[59] We also note that the exposure temperature used here is too high to allow occupancy of the multilayer region and weakly binding external sites observed by Ulbricht. This is consistent with the observation that our saturation experiments (not shown) were well below the saturation coverage observed by Kuznetsova et al.[60] and Ulbricht.[59]

The present results for adsorption potentials $V(\mathbf{r})$ may be compared with those derived from the more traditional "pairwise summation" approach. The latter approach, which we describe with the term "classical", is based on the *ansatz*

$$V(\mathbf{r}) = \sum_j U_{aC}(\mathbf{r}, \mathbf{R}_j) \tag{2}$$

where $\mathbf{R}_j$ is the position of the j-th carbon atom, a is the adsorbed atom (e.g., Ar) at position $\mathbf{r}$, and C represents each carbon atom in the adsorbent. The pair potential $U_{aC}(\mathbf{r}, \mathbf{R}_j)$ is usually taken to depend on just the magnitude $|\mathbf{r} - \mathbf{R}_j|$ of the adatom−C atom separation vector, $(\mathbf{r} - \mathbf{R}_j)$, which implicitly assumes that both the adatom and C atom are isotropic. That assumption is certainly not valid when dealing with sp^2-bonded carbonaceous materials, such as graphite and fullerenes. For example, the static polarizability tensor α_{jk} of the C atoms in graphite is quite anisotropic; the in-plane (diagonal) matrix elements $\alpha_{xx} = \alpha_{yy}$ are larger by a factor ~3.5 than the element α_{zz} along the c axis.[61] This anisotropy has a significant effect on the adatom−C vdW interaction, $U_{aC}(\mathbf{r}, \mathbf{R}_j)$.[62] Thus, the attractive (vdW) part of this potential is expected ab initio to depend on $P_2 \cos\theta$, where θ is the angle between the vector $(\mathbf{r} - \mathbf{R}_j)$ and the surface normal. The use of such *anisotropic* potentials in describing physisorption began when it was found that isotropic pair potentials were not consistent with extensive He−graphite scattering data,[63−65] while anisotropic potentials were consistent.[66,67] The key difference was the presence of larger corrugation in the latter case, required to explain the larger diffraction implied by the experimental scattering data. Anisotropic potentials have also been found to be consistent with the thermodynamic properties of He on graphite.[68−70] For other gases on graphite, the evidence for anisotropic potentials is much less extensive because there are no corresponding scattering data.

The form taken for Lennard−Jones-based anisotropic potentials is[71]

$$\frac{U_{aC}(x)}{4\varepsilon_{aC}} = \left(\frac{\sigma_{aC}}{x}\right)^{12}\{1 + \gamma_R[1 - (6/5)\cos^2\theta]\} - \left(\frac{\sigma_{aC}}{x}\right)^{6}\{1 + \gamma_A[1 - (3/2)\cos^2\theta]\} \tag{3}$$

Here, x is the scalar distance between an adatom "a" interacting with a C atom in the SWNT. The Lennard−Jones parameters, ε_{aC} and σ_{aC}, are derived from the usual Lorentz−Berthelot combining rules, while $\gamma_A = -0.38$ and $\gamma_R = -0.54$ are the attractive and repulsive anisotropic interaction parameters, respectively, assumed to be independent of the adatom type. The numerical values were derived for the case of He on graphite.[66,67]

Kim et al.[71] recently used this model potential in Monte Carlo simulations to predict the behavior of Ar and Kr films on a single isolated nanotube. Their results for Ar were in relatively good agreement with experimental results of Wang et al.,[72] who measured the coverage of Ar and Kr on a single suspended SWNT as a function of gas pressure. The coverage was determined in this remarkable experiment from the frequency shift of the oscillatory resonance of a single nanotube, due to adsorption from the coexisting gas vapor.[72] However, there was a qualitative difference between the predictions and the experimental results for Kr, as manifested by a discontinuity in the experimental isotherms.[72] The experimental data were interpreted in terms of a $\sqrt{3} \times \sqrt{3}$ R30° commensurate monolayer on the nanotubes, which is known to be a very prominent phase of Kr on graphite.[73] In contrast, the calculations yielded a different commensurate phase, of 50% higher density, in both the adsorption simulation results and in ground-state calculations for Kr. In such a phase, one-half of the Kr atoms occupy less energetically favored bridge site positions for the sake of more advantageous Kr−Kr interaction energy. This disagreement motivates us to compare results from this semiempirical, classical method with those derived from the present vdW-DF2 method.

Figure 8 presents interaction potentials from classical and vdW-DF2 calculations for a (20, 0) nanotube with Ar and Kr. The classical potentials were computed from eq 3 using ε_{ArC} = 57.97 K, σ_{ArC} = 3.4 Å, ε_{KrC} = 69.20 K, and σ_{KrC} = 3.5 Å. In both cases, the vdW-DF2 result is some 12−15 meV more attractive than the corresponding classical potentials; the equilibrium distances are approximately 0.1−0.2 Å farther away from the SWNT surface in the vdW-DF2 potential than in the classical potential. However, the corrugations are seen to be relatively similar in the two very different kinds of calculations. For

dx.doi.org/10.1021/ja402928s | J. Am. Chem. Soc. 2013, 135, 7768−7776

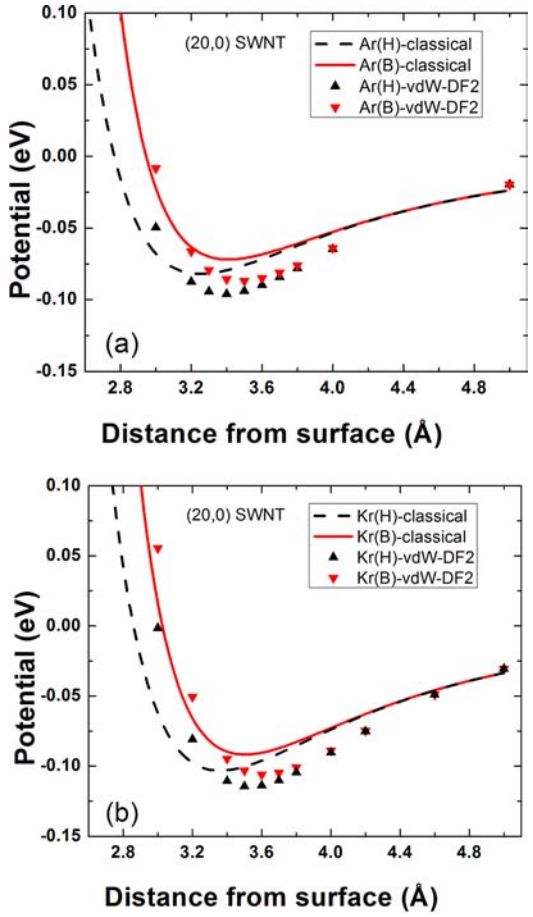

Figure 8. Potential energy curves for (a) Ar and (b) Kr as a function of the radial distance from the surface of a (20, 0) SWNT, as computed from vdW-DF2 (points) and classical potentials (curves). H and B denote the hexagon and bridge sites, respectively.

example, for Ar, the depth of the potential minimum radially outward from the hollow site (denoted H) differs from that above the bridge site (denoted B) by about 10 meV in the classical calculations and by 9 meV in the vdW-DF2 results. For Kr, the numbers disagree by somewhat more (11 meV classically vs 8 meV in the vdW-DF2 method). These differences have implications for the comparison mentioned above with the experimental data.[72] First, the greater binding of the new potentials would imply a lower onset pressure for the formation of a monolayer film. In point of fact, for Kr at 77.4 K, the experimental film condenses at a somewhat lower pressure than predicted by the classical potential (i.e., at 0.06 vs 0.1 Torr).[71] This onset difference corresponds to the surface binding of an additional monolayer atom by $kT \ln(0.1/0.06) \sim$ 3.4 meV (i.e., excess above the classical prediction). The value computed from the difference between the potential well depths of the vdW-DF2 and classical potentials for Kr at the hollow site is 12 meV. This is in qualitative agreement with the experiments in that use of the vdW-DF2 potential will lead to a lower transition pressure than computed from the classical potential.

Our newer potentials also shed light on the relationship between the contradictory results cited above for experiment/simulation for the two commensurate phases. In particular, the smaller corrugation for the vdW-DF2 potential would suggest that the $\sqrt{3} \times \sqrt{3}$ R30° commensurate phase would be *even* less favored on the nanotube than the classical potential predicts. Since the classical potential strongly *disfavors* that phase, the new results are consistent with that earlier finding; that is, the new results suggest that the higher density phase is even more favored than Kim et al. predicted. Thus, the apparent discrepancy with the experimental data becomes even greater, if the new potential calculations are correct. Evidently, to make more quantitative statements about the phase behavior will require detailed simulations with the new potentials, which we intend to carry out in the near future.

4. CONCLUSION

A combined approach of theoretical calculations and experimental measurements has been utilized to understand the adsorption of noble gases and *n*-heptane adsorption on M- and S-SWNTs with similar diameters. The vdW-corrected DFT calculations and TPD experiments enable us to probe the dominant, but weak, vdW interaction between gases and SWNTs. We found virtually no differences between M- and S-SWNT desorption energies for Ar, Kr, and Xe, indicating that the large difference between M- and S-SWNT static polarizabilities does not affect the adsorption. The vdW-corrected DFT method based desorption energies of Xe are in good agreement with measured desorption temperatures.

The conclusion for small atoms holds true for the much larger molecule, *n*-heptane, that is, the calculated and measured desorption energies are almost the same for S- and M-SWNTs of similar diameters. Our results can be rationalized by noting that the anomalous vdW interactions arising from gapless $\pi_z \rightarrow \pi_z^*$ transitions are negligible near the potential minimum.[74] Our results shed light on gas adsorption on M- and S-SWNTs, where no difference of vdW energy should be observed. It is expected that this conclusion should apply to all cases where the interaction between an adsorbate and (either M- or S-) SWNTs is dominated by vdW interactions. This is also helpful in understanding the mechanism of separation of S- and M-SWNTs by physisorption of large molecules,[17,18] i.e., the difference in adsorption of surfactant molecules on M- and S-SWNTs is likely not from differences in the vdW energy but due to some other contribution, for example, charge transfer.

■ AUTHOR INFORMATION

Corresponding Author

karlj@pitt.edu; johnt@virginia.edu

Notes

The authors declare no competing financial interest.

■ ACKNOWLEDGMENTS

This material is based upon work supported by the Department of Energy under Award Number DE-SC0004484 and by DTRA under Contract Number HDTRA1-09-1-0008. Calculations were performed at the University of Pittsburgh Center for Simulation and Modeling. We thank Hye-Young Kim for the classical potential calculations and John Dobson for several discussions of van der Waals interactions.

■ REFERENCES

(1) Hamada, N.; Sawada, S.-i.; Oshiyama, A. *Phys. Rev. Lett.* **1992**, *68*, 1579−1581.
(2) Ouyang, M.; Huang, J.-L.; Lieber, C. M. *Acc. Chem. Res.* **2002**, *35*, 1018−1025.
(3) Joselevich, E.; Lieber, C. M. *Nano Lett.* **2002**, *2*, 1137−1141.
(4) Kozinsky, B.; Marzari, N. *Phys. Rev. Lett.* **2006**, *96*, 166801.

(5) Lu, W.; Wang, D.; Chen, L. *Nano Lett.* **2007**, *7*, 2729−2733.
(6) Yanagi, K.; Udoguchi, H.; Sagitani, S.; Oshima, Y.; Takenobu, T.; Kataura, H.; Ishida, T.; Matsuda, K.; Maniwa, Y. *ACS Nano* **2010**, *4*, 4027−4032.
(7) Chang, D. B.; Cooper, R. L.; Drummond, J. E.; Young, A. C. *Phys. Lett.* **1971**, *37A*, 311−312.
(8) Dobson, J. F.; White, A.; Rubio, A. *Phys. Rev. Lett.* **2006**, *96*, 073201.
(9) Jhi, S.-H.; Louie, S. G.; Cohen, M. L. *Phys. Rev. Lett.* **2000**, *85*, 1710−1713.
(10) Zhao, J. J.; Buldum, A.; Han, J.; Lu, J. P. *Nanotechnology* **2002**, *13*, 195−200.
(11) Collins, P. G.; Bradley, K.; Ishigami, M.; Zettl, A. *Science* **2000**, *287*, 1801−1804.
(12) Zheng, M.; Jagota, A.; Semke, E. D.; Diner, B. A.; Mclean, R. S.; Lustig, S. R.; Richardson, R. E.; Tassi, N. G. *Nat. Mater.* **2003**, *2*, 338−342.
(13) Zhao, J. J.; Lu, J. P.; Han, J.; Yang, C. K. *Appl. Phys. Lett.* **2003**, *82*, 3746−3748.
(14) Lu, J.; Nagase, S.; Zhang, X. W.; Wang, D.; Ni, M.; Maeda, Y.; Wakahara, T.; Nakahodo, T.; Tsuchiya, T.; Akasaka, T.; Gao, Z. X.; Yu, D. P.; Ye, H. Q.; Mei, W. N.; Zhou, Y. S. *J. Am. Chem. Soc.* **2006**, *128*, 5114−5118.
(15) Strano, M. S.; Dyke, C. A.; Usrey, M. L.; Barone, P. W.; Allen, M. J.; Shan, H. W.; Kittrell, C.; Hauge, R. H.; Tour, J. M.; Smalley, R. E. *Science* **2003**, *301*, 1519−1522.
(16) Tournus, F.; Charlier, J. C. *Phys. Rev. B* **2005**, *71*, 165421.
(17) Arnold, M. S.; Green, A. A.; Hulvat, J. F.; Stupp, S. I.; Hersam, M. C. *Nat. Nanotechnol.* **2006**, *1*, 60−65.
(18) Antaris, A. L.; Seo, J. W. T.; Green, A. A.; Hersam, M. C. *ACS Nano* **2010**, *4*, 4725−4732.
(19) Chen, D. L.; Al-Saidi, W. A.; Johnson, J. K. *Phys. Rev. B* **2011**, *84*, 241405.
(20) Chen, D. L.; Al-Saidi, W. A.; Johnson, J. K. *J. Phys.: Condens. Matter* **2012**, *24*, 414211.
(21) Foulkes, W. M. C.; Mitas, L.; Needs, R. J.; Rajagopal, G. *Rev. Mod. Phys.* **2001**, *73*, 33−83.
(22) Lebegue, S.; Harl, J.; Gould, T.; Angyan, J. G.; Kresse, G.; Dobson, J. F. *Phys. Rev. Lett.* **2010**, *105*, 196401.
(23) Olsen, T.; Yan, J.; Mortensen, J. J.; Thygesen, K. S. *Phys. Rev. Lett.* **2011**, *107*, 156401.
(24) Dion, M.; Rydberg, H.; Schröder, E.; Langreth, D. C.; Lundqvist, B. I. *Phys. Rev. Lett.* **2004**, *92*, 246401.
(25) Rométez-Pérez, G.; Soler, J. *Phys. Rev. B* **2009**, *103*, 096102.
(26) Lee, K.; Murray, É. D.; Kong, L.; Lundqvist, B. I.; Langreth, D. C. *Phys. Rev. B* **2010**, *82*, 081101.
(27) Tkatchenko, A.; Scheffler, M. *Phys. Rev. Lett.* **2009**, *102*, 073005.
(28) Al-Saidi, W. A.; Voora, V. K.; Jordan, K. D. *J. Chem. Theory Comput.* **2012**, *8*, 1503−1513.
(29) Lee, K.; Kelkkanen, A. K.; Berland, K.; Andersson, S.; Langreth, D. C.; Schröder, E.; Lundqvist, B. I.; Hyldgaard, P. *Phys. Rev. B* **2011**, *84*, 193408.
(30) Ma, J.; Michaelides, A.; Alfè, D.; Schimka, L.; Kresse, G.; Wang, E. *Phys. Rev. B* **2011**, *84*, 033402.
(31) Chen, D.-L.; Mandeltort, L.; Saidi, W. A.; Yates, J. T., Jr.; Cole, M. W.; Johnson, J. K. *Phys. Rev. Lett.* **2013**, *110*, 135503.
(32) NanoIntegris, 2011.
(33) Guo, T.; Nikolaev, P.; Thess, A.; Colbert, D. T.; Smalley, R. E. *Chem. Phys. Lett.* **1995**, *243*, 49−54.
(34) Rinzler, A.; Liu, J.; Dai, H.; Nikolaev, P.; Huffman, C.; Rodriguez-Macias, F.; Boul, P.; Lu, A.; Heymann, D.; Colbert, D.; Lee, R.; Fischer, J.; Rao, A.; Eklund, P.; Smalley, R. *Appl. Phys. A: Mater. Sci. Process.* **1998**, *67*, 29−37.
(35) Kondratyuk, P.; Yates, J. T., Jr. *Acc. Chem. Res.* **2007**, *40*, 995−1004.
(36) Peigney, A.; Laurent, C.; Flahaut, E.; Bacsa, R. R.; Rousset, A. *Carbon* **2001**, *39*, 507−514.
(37) Kondratyuk, P.; Yates, J. T., Jr. *J. Vac. Sci. Technol., A* **2005**, *23*, 215−217.
(38) Yates, J. T., Jr. *Experimental Innovations in Surface Science*; Springer-Verlag: New York, 1997.
(39) Miller, J. B.; Siddiqui, H. R.; Gates, S. M.; Russell, J. N., Jr.; Yates, J. T., Jr.; Tully, J. C.; Cardillo, M. J. *J. Chem. Phys.* **1987**, *87*, 6725−6732.
(40) Bondi, A. *J. Chem. Eng. Data* **1963**, *8*, 371−381.
(41) Kresse, G. *J. Non-Cryst. Solids* **1995**, *193*, 222−229.
(42) Kresse, G.; Hafner, J. *Phys. Rev. B* **1994**, *49*, 14251−14269.
(43) Kresse, G.; Furthmuller, J. *Phys. Rev. B* **1996**, *54*, 11169−11186.
(44) Kresse, G.; Furthmuller, J. *Comput. Mater. Sci.* **1996**, *6*, 15−50.
(45) Klimeš, J.; Bowler, D. R.; Michaelides, A. *Phys. Rev. B* **2011**, *83*, 195131.
(46) Monkhorst, H. J.; Pack, J. D. *Phys. Rev. B* **1976**, *13*, 5188−5192.
(47) Kondratyuk, P.; Wang, Y.; Johnson, J. K.; Yates, J. T., Jr. *J. Phys. Chem. B* **2005**, *109*, 20999−21005.
(48) Kondratyuk, P.; Yates, J. T., Jr. *Chem. Phys. Lett.* **2005**, *410*, 324−329.
(49) Kondratyuk, P.; Yates, J. T., Jr. *J. Am. Chem. Soc.* **2007**, *129*, 8736−8739.
(50) Yates, J. T., Jr. In *Methods in Experimental Physics*; Park, R. L., Lagally, M. G., Eds.; Academic Press: Waltham, MA, 1985; Vol. *22*, pp 425−464.
(51) Redhead, P. A. *Vacuum* **1962**, *12*, 203−211.
(52) Tait, S. L.; Dohnalek, Z.; Campbell, C. T.; Kay, B. D. *J. Chem. Phys.* **2006**, *125*, 234308−234315.
(53) Becker, K. E.; Fichthorn, K. A. *J. Chem. Phys.* **2006**, *125*, 184706−184709.
(54) Gellman, A. J.; Paserba, K. R. *J. Phys. Chem. B* **2002**, *106*, 13231−13241.
(55) Paserba, K. R.; Gellman, A. J. *Phys. Rev. Lett.* **2001**, *86*, 4338−4341.
(56) Pussi, K.; Smerdon, J.; Ferralis, N.; Lindroos, M.; McGrath, R.; Diehl, R. D. *Surf. Sci.* **2004**, *548*, 157−162.
(57) Da Silva, J. L. F.; Stampfl, C. *Phys. Rev. B* **2007**, *76*, 085301.
(58) Sheng, L.; Ono, Y.; Taketsugu, T. *J. Phys. Chem. C* **2010**, *114*, 3544−3548.
(59) Ulbricht, H. *Surf. Sci.* **2009**, *603*, 1853−1862.
(60) Kuznetsova, A.; Yates, J. J. T.; Liu, J.; Smalley, R. E. *J. Chem. Phys.* **2000**, *112*, 9590−9598.
(61) Phillips, J. C. *Covalent Bonding in Crystals, Molecules and Polymers*; University of Chicago Press: Chicago, IL, 1969.
(62) Margenau, H. J.; Kestner, N. R. *Theory of Intermolecular Forces*; Pergamon: London, 1969.
(63) Boato, G.; Cantini, P. In *Advances in Electronics and Electron Physics*; Peter, W. H., Ed.; Academic Press: Waltham, MA, 1983; Vol. *60*, pp 95−160.
(64) Derry, G.; Wesner, D.; Vidali, G.; Thwaites, T.; Frankl, D. R. *Surf. Sci.* **1980**, *94*, 221−231.
(65) Boato, G.; Cantini, P.; Tatarek, R.; Felcher, G. P. *Surf. Sci.* **1979**, *80*, 518−523.
(66) Carlos, W. E.; Cole, M. W. *Surf. Sci.* **1980**, *91*, 339−357.
(67) Carlos, W. E.; Cole, M. W. *Phys. Rev. Lett.* **1979**, *43*, 697−700.
(68) Dash, J. G.; Schick, M.; Vilches, O. E. *Surf. Sci.* **1994**, *299−300*, 405−414.
(69) Corboz, P.; Boninsegni, M.; Pollet, L.; Troyer, M. *Phys. Rev. B* **2008**, *78*, 245414.
(70) Pierce, M. E.; Manousakis, E. *Phys. Rev. B* **2000**, *62*, 5228−5237.
(71) Kim, H.-Y.; Cole, M. W.; Mbaye, M.; Gatica, S. M. *J. Phys. Chem. A* **2011**, *115*, 7249−7257.
(72) Wang, Z.; Wei, J.; Morse, P.; Dash, J. G.; Vilches, O. E.; Cobden, D. H. *Science* **2010**, *327*, 552−555.
(73) Chinn, M. D.; Fain, S. C., Jr. *Phys. Rev. Lett.* **1977**, *39*, 146−149.
(74) Dobson, J. F.; Gould, T. *J. Phys.: Condens. Matter* **2012**, *24*, 073201.